New Synthetic Route for the Incorporation of Manganese Species into the Pores of MCM-48

Sinue Gómez,[†] Oscar Giraldo,[||] Luis Javier Garcés,[†] Josanlet Villegas,[†] and Steven L. Suib*[,†,‡,§]

Institute of Materials Science, Department of Chemistry, and Department of Chemical Engineering, University of Connecticut, Storrs, Connecticut 06269-3060 and Departamento de Física y Química, Universidad Nacional de Colombia, Manizales, Colombia

Received February 4, 2004. Revised Manuscript Received April 13, 2004

The present work describes a new way to synthesize manganese species within the channels of mesoporous MCM-48 silica using permanganate as manganese precursor agent. For the first time permanganate ions were incorporated within the as-synthesized mesoporous host by ion-exchange process. The resulting materials were characterized by XRD, N_2 sorption, transmission electron microscopy, EPR, XPS, Raman, and elemental analysis methods. The structure of the MCM-48 host material is maintained as indicated by XRD and HRTEM, and the surface areas of the MnMCM-48 materials are in the 670−930 m^2/g range compared to 1090 m^2/g for the host. The characterization results also indicate the presence of manganese species inside the silica pores, as well as a good dispersion of the manganese particles within the pores of the host material. Controlled manganese loading was possible to a maximum of 13 wt %. No bulk manganese was detected outside the MCM-48 mesoporous silica particles.

Introduction

The syntheses and studies of mesoporous materials with well-defined ordered structures have increased considerably in the past decade. Mesoporous materials have attracted the interest of both chemists and material scientists due to their broad range of applications. In 1992, a family of mesoporous silica materials was discovered by Mobil researchers and was designated as M41S.[1] These materials are formed by the assembly of long-chain surfactant organic molecules which act as structure-directing agents. This assembly is followed by the condensation of inorganic oxides that form extended thermally stable structures.[2] The most widely researched members of the M41S family are MCM-41 and MCM-48. MCM-41 consists of a hexagonal array and has an unidirectional pore structure, and MCM-48 consists of a cubic array with a three-dimensional pore network.[2] The unique pore system, high surface area (up to 1500 m^2/g), distinct adsorption properties, and high thermal stability make these materials good candidates for industrial applications. These properties of M41S materials make them attractive for applications such as adsorption and separation, ion-exchange, and in shape and size-selective applications such as catalysis, molecular sieves, and host structures for nanometer-sized compounds.[3−5] Nanomaterials are of special interest because of their catalytic, optical, and electronic properties. MCM-48 has been suggested to be a more advantageous system than MCM-41 for catalytic applications because the three-dimensional pore system of MCM-48 could allow faster diffusion through the channels as well as making it more resistant to pore blocking.[6]

The physical properties of M41S materials have encouraged the rapid development of new surface modification techniques. The incorporation of transition metals, such as Ti,[7−9] V,[7,9,10] Cr,[7,10,11] and Fe,[10,12−14] among others, into M41S materials using different synthetic routes has been studied extensively with the aim of developing new selective oxidation catalysts. Various authors have reported the incorporation of manganese species into the mesoporous M41S structures.[15−20] However, these methods have presented general problems

* To whom correspondence should be addressed. E-mail: suib@uconnvm.uconn.edu. Phone: (860) 486-2797. Fax: (860) 486-2981.
[†] Institute of Materials Science, University of Connecticut.
[‡] Department of Chemistry, University of Connecticut.
[§] Department of Chemical Engineering, University of Connecticut.
[||] Universidad Nacional de Colombia.

(1) Kresge, C. T.; Leonowicz, M. E.; Roth, W. J.; Vartulli, J. C.; Beck, J. S. *Nature* **1992**, *359*, 710.
(2) Ying, J. Y.; Mehnert, C. P.; Wong, M. S. *Angew. Chem., Int. Ed.* **1999**, *38*, 56.
(3) Corma, A. *Chem. Rev.* **1997**, *97*, 2373.
(4) Ciesla, U.; Schüth, F. *Microporous Mesoporous Mater.* **1999**, *27*, 131.
(5) Kang, K. K.; Ahn, W. S. *J. Mol. Catal. A: Chem.* **2000**, *159*, 403.
(6) Schumacher, K.; Ravikovitch, P. I.; Du Chesne, A.; Neimark, A. V.; Unger, K. K. *Langmuir* **2000**, *16*, 4648.
(7) Yuan, Z. Y.; Zhou, W.; Zhang, Z. L.; Liu, J. Q.; Wang, J. Z.; Li, H. X.; Peng, L. M. *Surf. Interface Catal.* **2001**, *32*, 193.
(8) Aronson, B. J.; Blanford, C. F.; Stein, A. *Chem. Mater.* **1997**, *9*, 2842.
(9) Lang, N.; Delichere, P.; Tuel, A. *Microporous Mesoporous Mater.* **2002**, *56*, 203.
(10) Pak, C.; Haller, G. L. *Microporous Mesoporous Mater.* **2001**, *48*, 165.
(11) Reddy, E. P. *J. Phys. Chem. B* **2002**, *106*, 3394.
(12) Fröba, M.; Köhn, R.; Gaellë, B. *Chem. Mater.* **1999**, *11*, 2858.
(13) Stockenhuber, M.; Joyner, R. W.; Dixon, J. M.; Hudson, M. J.; Grubert, G. *Microporous Mesoporous Mater.* **2001**, *44−45*, 367.
(14) Bourlinos, A. B.; Karakassides, M. A.; Petridis, D. *J. Phys. Chem. B* **2000**, *104*, 4380.
(15) Zhao, D. Y.; Goldfarb, D. J. *J. Chem. Soc., Chem. Commun.* **1995**, 875.
(16) Yonemitsu, M.; Tanaka, Y.; Iwamoto, M. *Chem. Mater.* **1997**, *9*, 2679.

10.1021/cm040018z CCC: $27.50
Published on Web 05/19/2004

which include the loss of the ordered mesoporous structure, low metal loadings, or formation of bulk species outside the silica host. Some of the more recent developments in the incorporation of manganese in M41S materials that have overcome some of these problems are the template ion-exchange method (TIE) reported by Yonemitsu and co-workers,[16] molecular organic chemical vapor deposition (MOCVD),[20] or the incorporation of Mn complexes by anchoring functional groups to the silica surface.[21]

In this work, MCM-48 will be used as a mesoporous host for manganese species using potassium permanganate as the manganese precursor. Permanganate precursors have been used previously in postsynthesis incorporation, using wet impregnation methods.[15] However, the amount of manganese introduced into the structure and the efficiency of the incipient wetness method is poor. This process decreases the order and the surface area of the host material and forms bulk manganese oxide outside the mesoporous silica particles.

The present work reports for the first time permanganate ions being incorporated into surfactant-containing mesoporous silica pores. The possibility of introducing permanganate ions into MCM-48 materials opens new opportunities for further synthesis of manganese oxide materials in confined environments and their use in catalytic applications. The method described in this work is a simple and new approach for the synthesis of manganese species in mesoporous silica materials.

Experimental Section

Synthesis of MCM-48. MCM-48 mesoporous silica was synthesized following a variation of the procedure described by Fröba and co-workers.[12] The synthesis mixture had the molar ratios 1:0.65:0.5:62 tetraethyl orthosilicate (TEOS)/cetyltrimethylammonium bromide (CTAB)/KOH/H_2O. The synthesis mixture was stirred for about 20 min and then loaded into a Teflon-lined steel autoclave where the synthesis solution was statically heated for 5 days at 115 °C. The resultant white precipitate was filtered, washed with deionized water, and dried at room temperature. After drying, the material was calcined in a furnace for 6 h at 550 °C.

Synthesis of MnMCM-48. Potassium permanganate ($KMnO_4$) was used as a manganese precursor to load manganese into the pores of MCM-48. Samples with different manganese contents were prepared using $KMnO_4$ with concentrations of 0.1, 0.05, and 0.005 M. In a typical loading procedure, approximately 100 mg of as-synthesized MCM-48 (surfactant-containing MCM-48) were slurried in water. Approximately 20 mL of $KMnO_4$ (0.05 M) was added to the slurry and the mixture was stirred for 4 h. Then the permanganate-containing MCM-48 was filtered, washed with deionized water, and dried at room temperature. The resulting purple product was calcined for 6 h at 550 °C. Samples with different manganese content are referred to as MnMCM-48(l), MnMCM-48(m), and MnMCM-48(h) for low, medium, and high content of manganese, respectively.

Characterization. The powder X-ray diffraction (XRD) patterns of the as-synthesized and calcined samples were recorded with a Scintag XDS-2000 diffractometer utilizing Cu Kα radiation with a voltage of 45 kV and current of 40 mA. N_2 sorption experiments were performed to obtain the surface areas and pore size distributions of the materials. The experiments were recorded in a Micrometrics ASAP 2010 analyzer. The samples were degassed at 150 °C overnight prior to data collection. The surface areas were calculated by applying the Brunauer−Emmett−Teller (BET) equation, and the pore size distribution was calculated using the desorption branch of the N_2 adsorption−desorption isotherm and the Barret−Joyner−Halenda (BJH) formula. Transmission electron microscopy (TEM) samples were prepared by dispersing the powder material in 2-propanol and placing a drop of the dispersion on a carbon-coated copper grid, then the alcohol was allowed to evaporate at ambient temperature. The high- resolution TEM (HRTEM) images and elemental analyses were taken with a JEOL 2010 coupled with an EDS unit. An inductively coupled plasma atomic emission spectrometer (ICP-AES) was used to determine the total content of manganese incorporated in the mesoporous silica. The samples were digested in HCl/HNO_3 overnight and diluted for analysis. ICP-AES was also used to determine the Si species released in the filtrate after incorporation of MnO_4^-. The average oxidation state (AOS) of manganese present in MnMCM-48 was determined from the values of total Mn content and active oxygen contents in MnO_x. Total Mn was estimated by a potentiometric titration employing a standard procedure for analysis of manganese in battery materials.[22] A detailed procedure for AOS calculations has been described elsewhere.[23,24] Ratios of $Mn^{2+}/Mn^{3+}/Mn^{4+}$ were determined by individual titrations as described by Parida et al.[25,26] Mn^{2+} was estimated by leaching a weighed amount of sample in $(NH_4)_2SO_4$ solution, followed by titration by the standard bismuthate method.[26] Mn^{4+} was determined by the standard arsenate reduction method.[26] Electron paramagnetic resonance (EPR) measurements were performed using X-band (9 GHz) EPR at 298 K on a Bruker EMX spectrometer. EPR samples were loaded into 3-mm o.d. by 2-mm i.d. quartz tubes. The Raman spectra were taken at room temperature in the spectral range 100−2000 cm^{-1} using a Renishaw 2000 Raman microscope system, which includes an optical microscope and a CCD camera for multichannel detection. The spectra were recorded using a 514-nm argon ion laser. X-ray photoelectron spectroscopy (XPS) data were collected on a Leybold-Heraeus (LH) model 10 spectrometer equipped with a SPECS EA10 MCD hemispherical analyzer. The samples were pressed in indium foil to minimize charging. Narrow and wide scans of all elements were collected for the prominent photoelectron transitions and X-ray excited Auger transitions.

Results

X-ray Diffraction. The XRD patterns obtained for calcined MCM-48 and MnMCM-48 with different loading materials are depicted in Figure 1. All the materials show the typical low-angle *hkl* reflections characteristic of the cubic space group *Ia*3*d*.[27] The overall mesoporous cubic structure after Mn incorporation is maintained; however, loss of peak intensities in the XRD pattern as Mn loading is increased is observed. The peak intensity

(17) Wang, L.; Shi, J.; Yu, J.; Yan, D. *Nanostruct. Mater.* **1998**, *10*, 1289.
(18) Xu, J.; Luan, Z.; Hartman, M.; Kevan, L. *Chem. Mater.* **1999**, *11*, 2928.
(19) Aronson, B. J.; Blanford, C. F.; Stein, A. *J. Phys. Chem. B* **2000**, *104*, 449.
(20) Caps, V.; Tsang, S. C. *Catal. Today* **2000**, *61*, 19.
(21) Evans, J.; Zaki, A. B.; El-Sheikh, M. Y.; El-Safty, S. A. *J. Phys. Chem. B* **2000**, *104*, 10271.
(22) Glover, D., Schumm, B., Jr., Kozowa, A., Eds. *Handbook of Manganese Dioxides Battery Grade*; International Battery Materials Association: Cleveland, Ohio, 1989.
(23) De Guzman, R.; Shen, Y. F.; Suib, S. L.; Shaw, B. R.; O'Young, C. L. *Chem. Mater.* **1993**, *5*, 1395.
(24) De Guzman, R. N.; Shen, Y. F.; Neth, E. J.; Suib, S. L.; O'Young, C. L.; Levine, S.; Newsam, J. M. *Chem. Mater.* **1994**, *6*, 815.
(25) Parida, K. M.; Kanungo, S. B.; Sant, B. R. *Electrochim. Acta* **1981**, *26*, 435.
(26) Vogel, A. I. *Vogel's Textbook of Quantitative Inorganic Analysis*; Longman Group Ltd.: Harlow, Essex, U.K., 1978; pp 606−607.
(27) Vartulli, J. C.; Schmitt, K. D.; Kresge, C. T.; Roth, W. J.; Leonowicz, M. E.; McCullen, S. B.; Hellring, S. D.; Beck, J. S.; Schlenker, J. L.; Olsen, D. H.; Sheppard, E. W. *Chem. Mater.* **1994**, *6*, 2317.

Table 1. Comparative Table of Results from XRD and N_2 Sorption Experiments

sample	d_{211} (Å)	shrinkage (%)[b]	BET surface area (m^2/g)	pore volume (cm^3/g)[c]	desorption pore diameter[d] (Å)
MCM-48	34.6 (39.6)[a]	14	1090	0.88	24.4
MnMCM-48(l)	35.3	11	930	0.86	25.0
MnMCM-48(m)	35.8	9	870	0.79	26.7
MnMCM-48(h)	36.4	8	670	0.65	27.2
MnMCM-48(m)[e]	36.9	n.a.[f]	980	0.85	27.0

[a] The value in parentheses is the d_{211} of the as-synthesized MCM-48. [b] The % shrinkage is defined as the contraction of the framework after heating, based on the difference between d_{211} for the as-synthesized sample and d_{211} for the calcined samples. [c] Single-point pore volume at $P/P_o = 0.99$. [d] BJH desorption pore diameter. [e] After Mn removal with HCl. [f] n.a. not applicable.

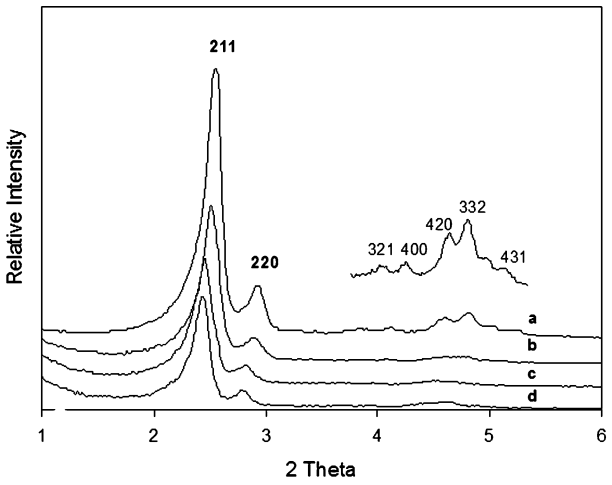

Figure 1. Powder XRD patterns of the calcined and as-synthesized samples (a) MCM-48, (b) MnMCM-48(l), (c) Mn−MCM-48(m), and (d) MnMCM-48(h).

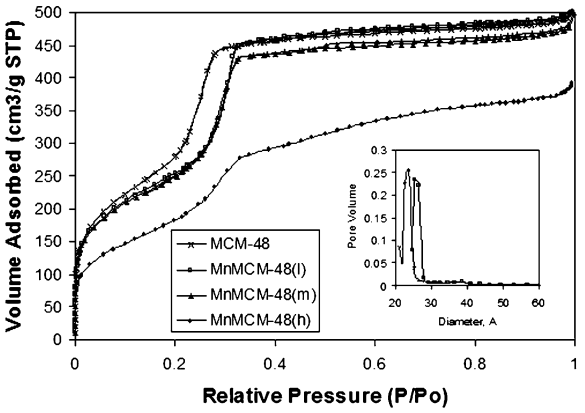

Figure 2. Nitrogen adsorption−desorption isotherms and BJH pore size distributions of calcined MCM-48 and MnMCM-48 with different manganese loadings.

can be reduced by random distribution of the guest particles in the channels, which would lower the periodicity.[19] The intensity decrease in the X-ray reflections with the incorporation of species into the pores can also be attributed to the partial collapse of the cubic ordered phase.[17,21] The d_{211} values as well as the percentage of shrinkage of the silica framework upon calcination are shown in Table 1. For the MnMCM-48 samples the d_{211} reflection peak shifts to lower 2θ values or larger d spacings when compared to the host material. Table 1 also shows the d spacings of the 211 reflection for MnMCM-48 with different Mn loadings. The d spacing of the calcined samples increases with increase of the Mn content, and the contraction of the silica walls decreases. These data indicate that as more Mn is present in the silica host the contraction of the silica walls in the calcination step decreases. No additional peaks due to manganese oxide phases are observed at high angles ($>5\theta$).

Nitrogen Sorption. Figure 2 and Table 1 show the N_2 sorption results obtained for the calcined MCM-48 and MnMCM-48 samples. The isotherms in all cases show type IV adsorption isotherms (IUPAC), typical of mesoporous materials.[28,29] The sharp inflection between relative pressure (P/P_o from 0.2 to 0.3) is due to capillary condensation of nitrogen within the pores. The sharpness of the inflection step reflects the uniform pore size distribution. The isotherms for all of the materials tested display reversible adsorption and desorption of nitrogen, as evidenced by the lack of hysteresis loops.

The amount of physisorbed nitrogen decreases with the loading of Mn, causing a reduction in surface area and pore volume; however, the pore size does not change drastically, as observed in Table 1. Even though the BHJ method is widely used to calculate the pore size in mesoporous materials, accuracy is limited because this method underestimates the calculated pore size in M41S materials by ~1 nm.[4,6] Thus, the pore size calculations in this case are used as a reference for changes in pore size. As can be seen in Table 1, removal of the Mn with HCl from the MnMCM-48(m) causes the surface area and the pore volume of the material to increase.

Electron Microscopy and EDS. The HRTEM micrograph and EDS spectrum for MnMCM-48 are shown in Figure 3. The structure of the mesoporous MCM-48 host seems not to be affected by the presence of manganese within the pores. The ordered cubic structure of the host material is maintained as can be seen in Figure 3, and the typical pattern corresponding to the projection along the [110] direction is observed.[30] No bulk manganese or precipitates outside the silica particles were found, however, a strong signal for manganese in the EDS data demonstrates that Mn is present. Additionally, no manganese agglomerates were observed with elemental mapping.

Average Oxidation State and Elemental Analysis. The AOS of Mn in MnMCM-48 samples and the $Mn^{2+}/Mn^{3+}/Mn^{4+}$ molar ratios were determined, and the results are shown in Table 2. The Mn content as

(28) Sing, K. S. W.; Everet, D. H.; Haul, R. A. W.; Moscov, L.; Pierotti, R. A.; Rouquérol, J.; Siemieniewska, T. *Pure Appl. Chem.* **1985**, *57*, 603.
(29) Marler, B.; Oberhagemann, U.; Vortmann, S.; Gies, H. *Microporous Mater.* **1996**, *6*, 375.
(30) Alfredsson, V.; Anderson, M. W. *Chem. Mater.* **1996**, *8*, 1141.

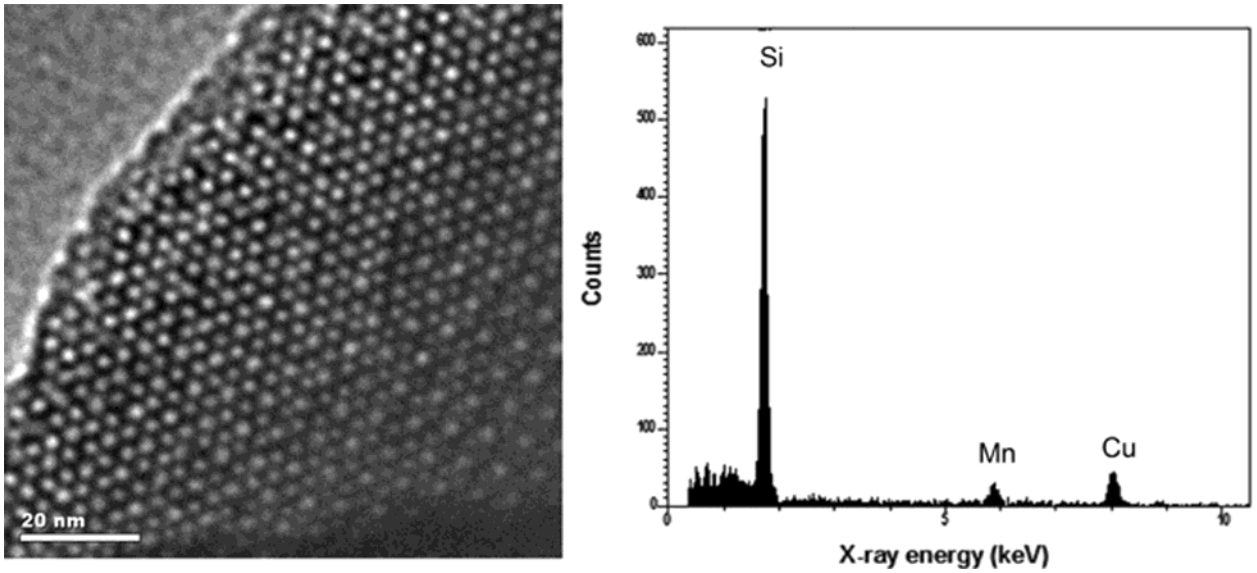

Figure 3. HRTEM images and EDS analyses for MnMCM-48(m). Cu is due to the sample grid.

Table 2. Total Manganese Content and AOS for the MnMCM-48 Samples

sample	total Mn content wt. %	$Mn^{4+}/Mn^{3+}/Mn^{2+}$	AOS
MnMCM-48(l)	3	1:0.36:0.10	3.6
MnMCM-48(m)	6	1:0.23:0.41	3.4
MnMCM-48(h)	13	1:0.22:0.49	3.3

determined by elemental analysis using ICP was 3, 6, and 13 wt. % for MnMCM-48(l), MnMCM-48(m), and MnMCM-48(h), respectively. The loss of Mn after stirring MnO_4^- containing MCM-48 in deionized water was only 7 wt % of the total content of manganese in the sample with medium content of manganese.

Electron Paramagnetic Resonance (EPR). The EPR spectra of the MnMCM48 materials with different Mn concentrations are depicted in Figure 4. At room-temperature all the samples show a signal centered at $g = 2.0$. Six well-resolved hyperfine lines are observed for the sample with lower Mn content. The six hyperfine lines originate from Mn^{2+} coupled to its own nuclear spin (^{55}Mn, $I_n = {}^5/_2$).[15,31] Because of significant zero field interaction the sextet lines are not equal in spacing and line height.[32] Then, by averaging the five separations of the hyperfine lines, an average hyperfine splitting constant of $A = 96$ G, is obtained. The *g*-factor and the hyperfine splitting constant obtained are characteristic of a Mn^{2+} complex in octahedral coordination.[18,31,32] The spectrum of the MnMCM-48(m) shows a poorly resolved hyperfine splitting, with $g = 2.0$ and $A = 96$ G; whereas for MnMCM-48(h) the signal broadens and is centered at $g = 2.0$. On the basis of similar EPR parameters obtained by other authors for Mn-containing MCM-41[31,33] and MCM-48[18] and in various zeolite materials,[34,35] the manganese species present in MnMCM-48 as determined by EPR can be assigned to extra framework sites of Mn^{2+} in octahedral symmetry.

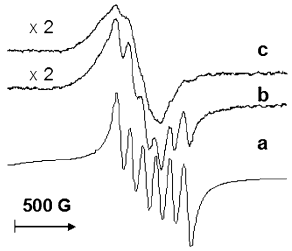

Figure 4. X-band EPR spectra at room temperature of calcined MnMCM-48 at (a) low, (b) medium, and (c) high manganese concentrations.

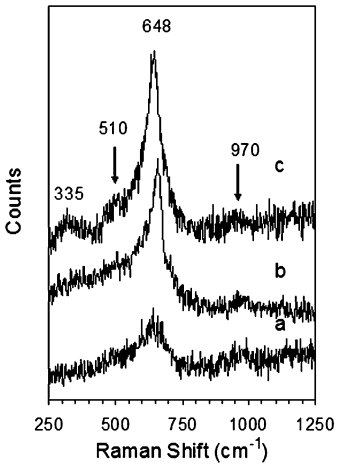

Figure 5. Raman spectra of MnMCM-48 at (a) low, (b) medium, and (c) high Mn concentrations.

Raman Spectroscopy. Raman spectroscopy was used to study the presence of Mn in the framework of the mesoporous silica. Various authors have used Raman techniques to study transition metal atoms in the framework of molecular sieves.[36−38] Figure 5 shows the Raman spectra for the MnMCM-48 samples. Weak Raman bands are observed at 510 and 970 cm^{-1}.

(31) Luan, Z.; Xu, J.; Kevan, L. *Chem. Mater.* **1998**, *10*, 3699.
(32) Xu, J.; Luan, Z.; Wasowicz, T.; Kevan, L. *Microporous Mesoporous Mater.* **1998**, *22*, 179.
(33) Zhang, J.; Goldfarb, D. *J. Am. Chem. Soc.* **2000**, *122*, 7034.
(34) Brouet, G.; Chen, X.; Lee, C. W.; Kevan, L. *J. Am. Chem. Soc.* **1992**, *114*, 3720.
(35) Levi, Z.; Raitsimring, A. M.; Goldfarb, D. *J. Phys. Chem.* **1991**, *95*, 7830.
(36) Zhang, Q.; Wang, Y.; Itsuki, S.; Shishido, T.; Takehira, K. *J. Mol. Catal. A: Chem.* **2002**, 188, 189.
(37) Geidel, E.; Lechert, H.; Döbler, J.; Jobic, H.; Calzaferri, G.; Bauer, F. *Microporous Mesoporous Mater.* **2003**, *65*, 31.
(38) Li, C. *J. Catal.* **2003**, *216*, 203.

Table 3. XPS Data for MnMCM-48(m)

element/orbital	binding energy (eV)	atomic concn (%)	assignment
Si 2p	102.94	34.84	SiO_2
O 1s	532.51	57.50	SiO_2
Mn $2p_{3/2}$/Mn $2p_{1/2}$	641.52/652.78	4.6	MnO_x

According to the literature these bands can be associated with symmetric and asymmetric stretching modes of Si−O−Mn species in the framework.[36−38] A stronger band is observed in the range of 640−660 cm^{-1} for all the MnMCM-48 samples and a weak band at 335 cm^{-1} is also observed in the sample with higher Mn content. These bands can be associated with the Mn species present in the mesopores.[39,40] The intensity of the bands associated with Mn species in the pores increases in all the samples as the Mn content increases; however, the intensity of the bands of the Si−O−Mn stretching vibrations remains about the same in all the samples.

X-ray Photoelectron Spectroscopy (XPS). XPS was used to analyze the binding energy (BE) values and the atomic surface concentration of the corresponding elements present in MnMCM-48. As determined by XPS the binding energies for the Si 2p, Mn 2p, and O 1s are shown in Table 3. The BE values obtained for Si 2p and O 1s correspond with literature values for SiO_2 frameworks.[41] The values of BE for Mn 2p were of 652.78 and 641.52 eV for the $2p_{1/2}$ and $2p_{3/2}$, respectively. As reported in the literature, the typical BEs for Mn^{4+} are 642 eV, 641−642 eV for Mn^{3+}, and 640 eV for Mn^{2+}.[19,41,42] Other authors report values of BE for Mn $2p_{3/2}$ in Mn_3O_4 situated in the 641.3−641.4 eV domain and for Mn_2O_3 BE of 641.3−641.9.[43] Because of the differences in BE values from different reports, identification of the type of manganese oxides present in a mixed-valent system is difficult. The interpretation of XPS spectra of Mn species present in MnMCM-48 is complex. The values obtained for MnMCM-48 agree with those of mixed-valent manganese oxide systems.[19,44] The atomic concentration ratio of manganese in the surface of MnMCM-48(m) is very low (4.6%). Because XPS is a surface technique, the photoelectron peaks would depend strongly on the surface concentration of the atoms present, thus making the interpretation of the data respect to Mn more complicated.

Discussion

Effect of Mn Incorporation on the Properties of MCM-48. Stability of the MCM-48 framework was evaluated by comparing the XRD patterns of Mn-containing material with that of the parent MCM-48. The intensity of the reflection peaks upon Mn incorporation is reduced. The introduction of scattering material within the pores leads to an increased phase cancellation between scattering from the silica wall and the pore regions, reducing the scattering intensities of the Bragg reflections.[12,29] Therefore, the reduction in peak intensities in MnMCM-48 is attributed to the presence of manganese guest species within the mesoporous structure, rather than to the partial collapse of the ordered cubic phase. The decrease in peak intensities is related to the amount of Mn present in the host material. The more Mn that is incorporated, the less intense are the Bragg reflections. The fact that Mn-MCM-48 maintains a cubic structure was also evident in the HRTEM micrographs; thus, the process of loading manganese into the pores of MCM-48 does not cause deterioration in the cubic order of the pore structure of MCM-48.

The presence of the manganese species restricts contraction of the framework when the sample is calcined, because the silica walls show lower contraction as the Mn concentration increases. The presence of manganese within the pores seems to add support to the framework, increasing its thermal stability, and preventing some contraction of the structure upon heating. Thus, the more manganese present in the pores the more stability is provided to the MCM-48 framework. In Table 1, the *d* spacing of the 211 reflection shows lower values after calcination when the Mn loading is 3 wt. % compared to that of a loading of 13 wt. %. The parent material shows lower *d* spacing than the Mn-containing MCM-48. This is also evidenced from the BJH pore size results, as the MnMCM-48 samples show larger pore size than the parent material.

The synthetic method used in this work is effective for the introduction of manganese into MCM-48, avoiding the formation of bulk Mn outside the domains of the silica particles. HRTEM images show the absence of metal oxide phases or precipitates formed outside the pore structure, which is in agreement with XRD results, where no diffraction peaks of manganese oxide phases were found at high angle. As reported by other authors, when the MCM-48 has an average diameter of ∼30 Å, the manganese oxide particles formed within the pores are too small to produce X-ray reflections.[12] The silica channels were also observed by HRTEM. Although no Mn clusters or particles could be identified in the pores, EDS experiments demonstrate the presence of Mn. EDS results also indicate that Mn is well distributed wherever the silica particles are present.

The decrease in surface area relative to the increment of manganese content is in agreement with the fact that more manganese is incorporated in the mesoporous host;, however, the materials still show high surface area values, ranging from 960 m^2/g for low Mn loading to 670 m^2/g for high Mn loading. Despite the fact that a considerable amount of the surface area and pore volume is restored after manganese removal (Table 1), some structural changes must occur within the silica framework after manganese introduction that prevents the material from recovering its initial properties. Some Mn could be migrating from the silica inner surface to the framework or the process of removing the manganese from the pores with HCl could be causing partial collapse of the silica walls, thus reducing the surface area. The fact that removal of Mn from the framework causes the pore size to increase is also consistent with less contraction of the silica walls. Reversible adsorption and desorption of nitrogen are observed for all the

(39) Buciuman, F.; Patcas, F.; Craciun, R.; Dietrich, R. T. Z. *Phys. Chem. Chem. Phys.* **1999**, *1*, 185.
(40) Radhakrishnan, R.; Oyama, T. S.; Chen, J. G.; Asakura, K. *J. Phys. Chem. B* **2001**, *105*, 4245.
(41) Stakheev, A. Y.; Shpiro, E. S.; Apijok, J. *J. Phys. Chem.* **1993**, *97*, 5668.
(42) Cao, H.; Suib, S. L. *J. Am. Chem. Soc.* **1994**, *116*, 5334.
(43) Cracium, R.; Dulamita, N. *Ind. Eng. Chem. Res.* **1999**, *38*, 1357.
(44) Ardizzone, S.; Bianchi, C. L.; Tirelli, D. *Colloids Surf., As* **1998**, *134*, 305.

materials evaluated. These facts indicate that there is negligible obstruction of the pore channels even for the MnMCM-48 material.[45] The presence of surfactant in the pores when incorporating permanganate could be restricting the location of the Mn species to the silica walls inside the pores, avoiding obstruction of the channels. The idea of synthesizing metal oxides in the presence of surfactant species has been reported before.[8,16] Aronson and co-workers reported the synthesis of titanium oxide into MCM-41 in the presence of surfactant in the mesopores to avoid clogging of the channels.[8] The shape of the pores is not altered by the presence of manganese in the mesoporous host, as the shape of the isotherm remains unchanged after manganese incorporation. The Mn-containing MCM-48 still shows mesoporosity, thus indicating that the Mn species are coating the inner surface of the mesoporous structure rather than filling it completely. The fact that the reduction in surface area is low despite high amounts of manganese being incorporated into the mesoporous host could be indicating that Mn species are covering the inner walls of the pores.

Manganese Species MnMCM-48. EPR was used to evaluate the state of manganese in the mesoporous material. Increasing the Mn content results in higher amount of Mn^{2+} species present resulting in significant broadening of the hyperfine lines and considerable decrease in the resolution of the whole spectra. The broadening can be attributed to spin exchange interactions due to a decrease in the $Mn^{2+}-Mn^{2+}$ distance.[36] The ratio of Mn^{2+} with respect to Mn^{4+} is almost 5 times higher for MnMCM-48(h) as compared to MnMCM-48(l), which is consistent with EPR observations. The fraction of Mn^{2+} species present in MnMCM-48 can be assigned to isolated species located in extraframework sites with octahedral symmetry.[18,31,33−35] However, Mn^{3+} and Mn^{4+} are also present in the MnMCM48 materials, as shown in Table 2. The electron configuration of Mn^{4+} allows observation of an EPR spectrum,[46−48] however, Mn^{4+} has *g* values lower than 2. In our case most of the contribution to the EPR spectrum seems to come from Mn^{2+}. For Mn^{4+} the spin quantum number is $S = {}^3/_2$, thus, the EPR signal of 1 mol of Mn^{4+} is ${}^7/_3$ times the EPR signal of 1 mol of Mn^{2+}.[45] The presence of Mn^{3+} in similar systems has been mentioned before,[18,49] but Mn^{3+} is silent to conventional X-band or Q-band EPR because it has large zero field splitting.[18]

The AOS data for manganese in the MnMCM-48 samples are 3.6, 3.4, and 3.3 for the low, medium, and high Mn concentrations, respectively, which indicates that a mixture of manganese species with different oxidation states coexists in all the samples. Raman experiments showed bands in the region of 300−680 cm^{-1} associated with the presence of Mn oxide species. Buciuman et al.[39] found vibrational frequencies in the range of 650−680 cm^{-1} for α-Mn_2O_3, and a strong peak at about 650 cm^{-1} and weak peaks at 310−370 cm^{-1} for Mn_3O_4. Raman experiments do not provide enough information to conclude about the type of Mn oxide, however we can relate the bands with Mn−O bonds. On the other hand, the XPS results showed that the BE results obtained for MnMCM-48 are also consistent with mixed-valent Mn in manganese oxide systems.[42,44] The presence of six well resolved hyperfine lines has been detected in oxide systems before.[24,50−52] Cordischi and co-workers detected hyperfine structure in perovskite type materials, but only at low concentrations of Mn, where Mn^{2+} was a minor component.[43] The presence of Mn^{2+} ions in octahedral symmetry has also been detected with EPR in synthetic todorokites.[24,50]

As mentioned before, EPR results suggest that only extraframework Mn^{2+} is present. Xu and co-workers found five different extraframework Mn^{2+} species as well as framework Mn^{2+} species present in similar Mn-containing MCM-48 materials.[18] None of those species could be detected under the EPR experimental conditions used in this work. Raman results demonstrate that some Mn is incorporated in the framework, however the amount is limited, and does not depend on Mn content.

Incorporation of Manganese Species. The formation of M41S mesoporous materials consists of a cooperative assembly of periodic inorganic and surfactant species.[2] Several models have been proposed for the formation of mesoporous silicate materials under different surfactant−inorganic conditions.[50] The synthesis of the MCM-48 mesoporous host in this work involves direct co-condensation of anionic inorganic species with a cationic surfactant under basic conditions. The process is based on electrostatic interactions to assemble species in solution of the type S^+I^-,[53−55] where I^- is the negatively charged silica species, and S^+ is the alkyltrimethylammonium cation CTA^+. The silica precursor (TEOS) forms anionic silicate species in basic solution such as double 4-ring (D4R) silicate anions.[2,55] When the precursor solutions are combined, the multiply charged D4R silicate species compete with and ion-exchange for Br^- or OH^- surfactant counterions.[55] The D4R silicates anions are preferred to other silicates present in the form of monovalent monomers to compensate for access to the cationic surfactant headgroups.[55]

In the silicate−surfactant interface, the uncondensed material is composed of D4R silicate anions complexed with surfactant.[2,25] Therefore, the incorporation of permanganate ions must be occurring by an anion-exchange process of uncondensed D4R anions in the interface by MnO_4^-. Thus, the MnO_4^- locates between

(45) Yang, H.; Vovk, G.; Coombs, N.; Sokolov, I.; Ozin, G. A. *J. Mater. Chem.* **1998**, *8*, 743.
(46) Goldberg, D. P.; Tesler, J.; Krzystek, J.; Montalban-Garrido, A.; Brunel, L.; Barret, A. G. M.; Hoffman, B. M. *J. Am. Chem. Soc.* **1997**, *119*, 8722.
(47) Kakazey, M.; Ivanova, N.; Boldurev, Y.; Ivanov, S.; Sokolsky, G.; Gonzalez-Rodriguez, J. G.; Vlasova, M. *J. Power Sources* **2003**, *114*, 170.
(48) Stoyanova, R.; Gorova, M.; Zhecheva, E. *J. Phys. Chem. Solids* **2000**, *61*, 615.
(49) Kiljstra, W. S.; Poels, E. K.; Bliek, A.; Weckhuysen, B. M.; Schoonheydt, R. A. *J. Phys. Chem. B* **1997**, *101*, 309.
(50) Nicolas-Tolentino, E.; Tian, Z.; Zhou, H.; Xia, G.; Suib, S. L. *Chem. Mater.* **1999**, *11*, 1733.
(51) Cordischi, D.; Faticanti, M.; Minelli, G.; Occhiuzzi, M.; Porta, P. *Phys. Chem. Chem. Phys.* **2003**, *5*, 1467.
(52) Tian, Z.; Tong, W.; Wang, J.; Duan, N.; Krishnan, V. V.; Suib, S. L. *Science* **1997**, *276*, 926.
(53) Huo, Q.; Margolese, D. I.; Ciesla, U.; Feng, P.; Gier, T. E.; Sieger, P.; Leon, R.; Petroff, P. M.; Schüth, F.; Stucky, G. D. *Nature* **1994**, *368*, 317.
(54) Huo, Q.; Margolese, D. I.; Ciesla, U.; Demuth, D. G.; Feng, P.; Gier, T. E.; Sieger, P.; Firouzi, A.; Chmelka, B. F.; Schüth, F.; Stucky, G. D. *Chem. Mater.* **1994**, *6*, 1176.
(55) Firouzi, A.; Kumar, D.; Bull, L. M.; Besier, T.; Sieger, P.; Huo, Q.; Walker, S. A.; Zasadzinski, J. A.; Glinka, C.; Nicol, J.; Margolese, D.; Stucky, G. D.; Chmelka, B. F. *Science* **1995**, *267*, 1138.

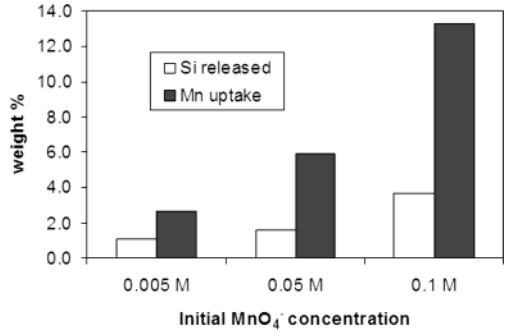

Figure 6. Representation of manganese uptake and silica species released after anion-exchange process with respect to initial concentration of the permanganate solution.

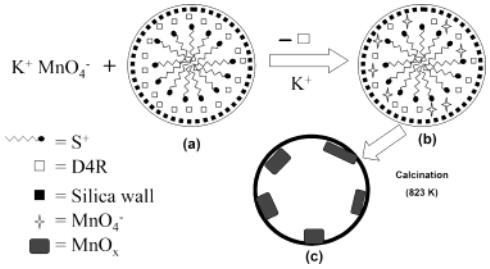

Figure 7. Schematic representation of the proposed mechanism for the process of incorporation of permanganate ions into the as-synthesized MCM-48: (a) represents the species coexisting in one pore of as-synthesized MCM-48, (b) represents one pore after ion-exchange of the D4R anionic species with permanganate ions, and (c) represents one pore after calcination.

S^+ and the silica walls, compensating electronic interactions in the structure. Figure 6 shows the manganese uptake and Si release after anion-exchange with respect to initial concentration of permanganate ions. The amount of Mn incorporated in the silica structure is around three times more than the amount of Si released. This observation is consistent with considering that the D4R species are multiply charged anions. A representative scheme of the process is depicted in Figure 7. Yonemitsu and co-workers developed a template ion-exchange method (TIE) using as-synthesized MCM-41.[16] The TIE method uses Mn^{2+} as precursor agent following a cation-exchange process where two template ions (1+ each ion) are replaced by one Mn^{2+} ion. In our method Mn^{7+} is used and a Mn mixed-valence system is obtained and allows high Mn loadings (13 wt. %).

When calcining the sample to remove the surfactant template, the manganese oxide particles seem to be located on the inner walls of the host and homogeneously distributed through the mesoporous silica structure. Because we assume the anion-exchange process of MnO_4^- species occurs only with species located in the pores between the silica wall and the surfactant species, there is no other place for the manganese species to locate, so that any excess of permanganate remained in the solution after the exchange takes place should be removed when the sample is filtered and washed, avoiding the formation of bulk manganese.

The stability of the permanganate ions in the silica structure for MnMCM-48(m) was tested by stirring the as-synthesized MnO_4^--containing MCM-48 in deionized water overnight at room temperature. The total manganese content measured after stirring in water showed only a 7 wt % loss of the total manganese content of the initial sample. This indicates that is not easy to remove the permanganate ions, and that they are stable within the silica pore structure.

Conclusions

In the present work we have successfully prepared manganese-containing MCM-48 using potassium permanganate as precursor agent by a simple method which follows an ion-exchange process. Using this method, it is possible to introduce different amounts of manganese into the mesoporous structure by simply varying the concentration of the initial permanganate solution. The amount of Mn incorporated is higher than with most procedures without damaging the properties of the parent material and avoiding the formation of bulk manganese oxide outside the porous structure. The XRD and TEM experiments demonstrate that the MCM-48 structure is maintained and strengthened by the presence of manganese species in the pores, thus increasing the thermal stability of the material. The TEM and EDS results together with XRD experiments confirm that manganese is present within the silica pores. N_2 sorption results indicate that a high surface area is maintained for MnMCM-48. EPR analysis confirms the presence of extraframework Mn^{2+} with octahedral coordination, and Raman shows some Mn is incorporated in the framework. The calculated AOS of the manganese species and XPS results indicate that manganese species exist in multiple oxidation states. To conclude, the method developed in this work, using permanganate (Mn^{7+}) with the aim of incorporating manganese species in mesoporous silica MCM-48, is simple and reproducible, and opens new trends for the in-situ synthesis of manganese oxides in confined environments.

Acknowledgment. We thank the U.S. Department of Energy, Geosciences and Biosciences Division, Office of Basic Energy Sciences, Office of Science, for financial support. We also thank the Institute of Materials Science and Dr. M. Aindow for providing access to electron microscopy facilities, Dr. K. Laubernds for the high resolution electron microscopy work, and Dr. Francis Galasso and Dr. Nelson Garcés for helpful discussions.

CM040018Z